Topological phase transitions induced by disorder in magnetically doped (Bi, Sb)$_2$Te$_3$ thin films

Takuya Okugawa [1], Peizhe Tang [2,3,*], Angel Rubio [3,4,5] and Dante M. Kennes [1,3,†]

[1]*Institut für Theorie der Statistischen Physik, RWTH Aachen, 52056 Aachen, Germany*
and JARA - Fundamentals of Future Information Technology, 52425 Jülich, Germany
[2]*School of Materials Science and Engineering, Beihang University, Beijing 100191, People's Republic of China*
[3]*Max Planck Institute for the Structure and Dynamics of Matter, Center for Free Electron Laser Science, 22761 Hamburg, Germany*
[4]*Center for Computational Quantum Physics, Simons Foundation Flatiron Institute, New York, New York 10010, USA*
[5]*Nano-Bio Spectroscopy Group, Departamento de Fisica de Materiales, Universidad del País Vasco, UPV/EHU- 20018 San Sebastián, Spain*

We study disorder induced topological phase transitions in magnetically doped (Bi, Sb)$_2$Te$_3$ thin films by using large scale transport simulations of the conductance through a disordered region coupled to reservoirs in the quantum spin Hall regime. Besides the disorder strength, the rich phase diagram also strongly depends on the magnetic exchange field, the Fermi level, and the initial topological state in the undoped and clean limit of the films. In an initially trivial system at nonzero exchange field, varying the disorder strength can induce a sequence of transitions from a normal insulating to a quantum anomalous Hall, then a spin-Chern insulating, and finally an Anderson insulating state. In contrast, for a system which is initially in the topological phase, a similar sequence can be induced by the disorder, but only starting from the quantum anomalous Hall phase that is also stabilized by the weak disorder. Varying the Fermi level we find a similarly rich phase diagram, including transitions from the quantum anomalous Hall to the spin-Chern insulating state via a state that behaves as a mixture of a quantum anomalous Hall and a metallic state, akin to recent experimental reports.

I. INTRODUCTION

The interplay between magnetism and topological states of matter has attracted tremendous research interests in the past decades for its value in both fundamental science and applications. Many interesting and exotic phenomena have been predicted and observed in these types of systems, such as antiferromagnetic (AFM) topological insulators (TIs) [1–3], AFM Dirac semimetals [4], and magnetic Weyl semimetals [5]. The observation of the quantum anomalous Hall (QAH) effect in two-dimensional (2D) topological materials, in which a dissipationless quantized Hall conductance carried by chiral edge states is found in transport measurements [6–9], is one of the most important contributions to this field. In contrast to the quantum Hall effect, the QAH effect does not necessitate any external magnetic field, but instead requires the spontaneous formation of long-range magnetic order inside the 2D materials which breaks the time reversal symmetry [6,10,11]. Currently, the QAH effect has been observed in twisted bilayer graphene [12,13], MnBi$_2$Te$_4$ thin film with an odd number of septuple layers [14], and magnetically doped TI thin film [6,7,15–22].

One of the first QAH material candidates, which have been well studied in the past few years, are magnetically doped TI thin films, such as Cr or V-doped (Bi, Sb)$_2$Te$_3$ with a thickness of several quintuple layers (QLs) [7,15–18].

Here, long-range ferromagnetic (FM) order is achieved by magnetic doping [6,7,10,11]. Once FM order is formed in these thin films, the strength of exchange field can be tuned efficiently by changing the concentration of magnetic ions and the chemical potential [10,23–26]. Furthermore, it was shown experimentally that electronic and topological properties of magnetically doped TI thin films can also be manipulated precisely via changing their thickness [27], tuning the chemical constituents [11], or applying a dual-gate technology [28,29].

The magnetically doped (Bi, Sb)$_2$Te$_3$ thin film can be regarded as an alloy structure, whose Bi sites are randomly occupied by doped magnetic atoms and Bi/Sb atoms at a certain percentage. Therefore, disorder effects are unavoidable in this kind of materials, and we can classify the disorder into two kinds. The one kind is magnetic disorder, e.g., induced by the magnetic dopands, that induces spin flips by scattering and breaks the time reversal symmetry. The other kind is nonmagnetic, does not break time reversal symmetry but does induce spatial inhomogeneity. For the first one, there are many recent studies [30–41], which conclude that weak magnetic disorder could stabilize a QAH effect and induce new topological phases, while strong disorder drives the system towards an Anderson insulator state. The second type of disorder has received less theoretical attention [42], although it is well known that spatial inhomogeneity of thin films is an important factor in experiments [20,38,39,43–46] (e.g., recent low temperature transport measurements in magnetically doped TI thin films have observed some scaling behavior of conductance, which is induced by the disorder effects [47])—a shortcoming that we will remedy within this Rapid Communication by focusing

_____
*peizhet@buaa.edu.cn
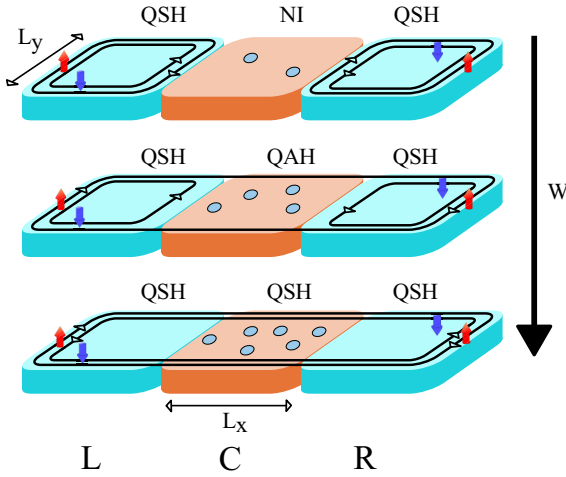†dante.kennes@rwth-aachen.de

FIG. 1. Schematic of the system. The QSH leads are given in light blue, while the central region is colored in orange. The disorder strength can tune a NI to a QAH and even to a QSH state as the disorder is varied. Depending on the phase the conductance is quantized to 0, 1, or 2 times the conductance quantum carried by edge states with locked pseudospin.

on this second type of disorder. This is particularly pressing as for intrinsic HgTe/CdTe quantum wells; this second type of disorder can induce a topological phase transition (TPT) driving the quantum well from a normal insulator (NI) to a topological Anderson insulator (TAI) with quantized edge conductance [48–52].

In this work, by using large scale tight-binding transport simulations of disordered 2D systems, we reveal the surprisingly rich phase diagram of magnetically doped TI thin films, which depends on the nondisordered (undoped) parent state in an intricate fashion. A schematic of our simulations is summarized in Fig. 1. We use a large central region exhibiting disorder of varying strength coupled to two semi-infinite leads. The transport via edge states through the central region depends on its topological phase and can be flexibly tuned by disorder strength. This finding is illustrated in detail in Figs. 2(a) and 2(b) for (Bi, Sb)$_2$Te$_3$ thin films with the thickness of 3QLs and 4QLs, hosting a NI and quantum spin Hall (QSH) state without disorder and exchange field, respectively. In dependence of the number of layers, disorder strength W and exchange field gM, a rich behavior of the topological phases is found by considering the conductance. Disorder can induce a series of transitions from NI → QAH → spin-Chern insulator → Anderson insulator as its strength is increased to larger values.

II. MODEL AND METHOD

We aim at modeling the electronic structures of magnetically doped (Bi, Sb)$_2$Te$_3$ thin films around the Fermi level at the Γ point by starting from the low-energy $\boldsymbol{k} \cdot \boldsymbol{p}$ effective Hamiltonian [6]:

$$H_0 = \begin{pmatrix} h(\boldsymbol{k}) + gM\sigma_z & 0 \\ 0 & h^*(\boldsymbol{k}) - gM\sigma_z \end{pmatrix}, \quad (1)$$
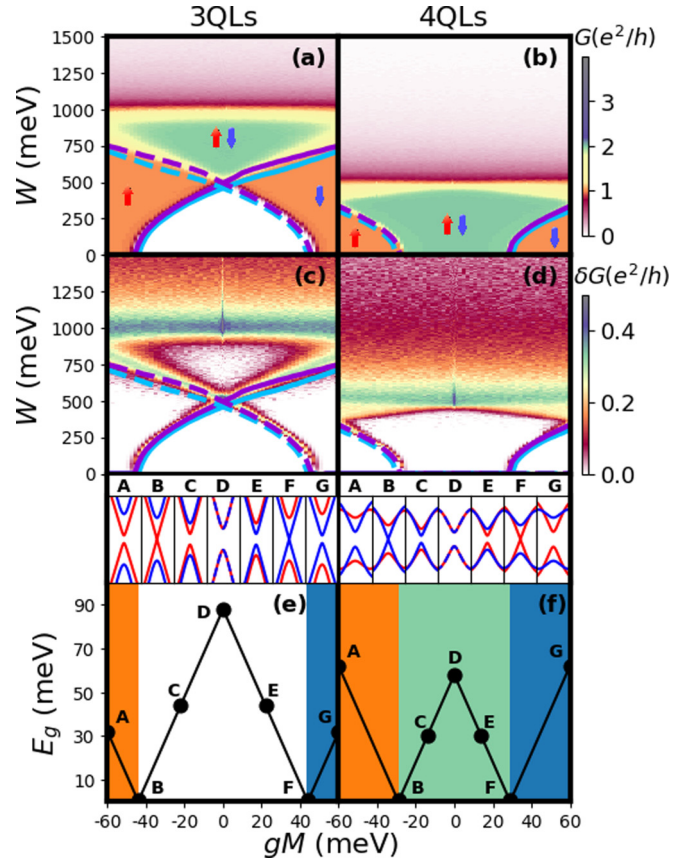

FIG. 2. Phase diagram of magnetically doped (Bi, Sb)$_2$Te$_3$ thin film with the thickness of 3QLs and 4QLs, corresponding to left and right column, respectively. Panels (a),(b) show the average conductance G and (c),(d) are the standard deviation δG as a function of the exchange field gM and disorder strength W. The system sizes are $L_x = 400a$ and $L_y = 100a$, a is the lattice constant. The Fermi level is 1 meV. The disorder average is taken over 500 random configurations. The red and blue spins indicate the pseudospins that distinguish the upper and lower block in Eq. (1). The colored lines represent the phase boundaries from self-consistent Born approximation. Details about the colored lines and the other parameters are given in Ref. [54]. (e) and (f) show the bulk band gap as a function of exchange field gM. The upper subpanels show bulk band sketches that correspond to the labeled points; the red (blue) lines represent the energy bands from the upper (lower) block in Eq. (1). The background color indicates different topological phases. Orange denotes a QAH insulator with Chern number $C = -1$, blue a QAH insulator with $C = +1$, green a spin-Chern insulator, and white a NI.

with $h(\boldsymbol{k}) = \boldsymbol{d}(\boldsymbol{k}) \cdot \boldsymbol{\sigma}$, $\boldsymbol{d}(\boldsymbol{k}) = (v_F k_y, -v_F k_x, m(\boldsymbol{k}))$ and $m(\boldsymbol{k}) = m_0 + B(k_x^2 + k_y^2)$. Here, the basis is chosen as $|+\uparrow\rangle$, $|-\downarrow\rangle$, $|+\downarrow\rangle$, $|-\uparrow\rangle$, where $|\pm\uparrow(\downarrow)\rangle = (|t\uparrow(\downarrow)\rangle \pm |b\uparrow(\downarrow)\rangle)/\sqrt{2}$, and $t(b)$ represents the top (bottom) surface states. $\boldsymbol{\sigma} = (\sigma_x, \sigma_y, \sigma_z)^T$ is a vector with the entries being the Pauli matrices for real spin ($\uparrow$ and $\downarrow$). v_F is the Fermi velocity, M is the exchange field in the z direction, and g is the effective g factor. $m(\boldsymbol{k})$ describes the tunneling between the top and the bottom surface, which goes to zero as the thickness of the film is increased. Since the Hamiltonian shown in Eq. (1) is block diagonal, topological properties and

the energy dispersion can be defined for each block of the Hamiltonian separately [53].

In order to quantify the effect of disorder on the magnetic TI, we perform transport calculations as a function of both disorder strength W and the effective exchange field gM. We use a lattice version of the Hamiltonian of Eq. (1) with quenched random onsite disorder uniformly distributed within $[-W/2, W/2]$ (see SM for details [55]). We then calculate the disorder averaged conductance G and the corresponding standard deviation δG of a stripe geometry using the Landauer-Büttiker formula [56,57]. A similar approach was applied to other topological materials showing a TAI phase [48–50]. Our stripe geometry consists of a disordered central region with the length L_x and width L_y connected to a left and right semi-infinite clean lead (see Fig. 1). In contrast to previous works we here suggest leads in the QSH regime to probe the conductance. This choice of leads, though not affecting the central region's physics (see SM [55]), allows us to probe the conductance much more clearly, and we suggest to use a similar setup in future experiments.

We compare our exact simulations on disorder induced TPT with a self-consistent Born approximation [49], in which the effect of disorder can be subsumed in a change of the topological mass term and the chemical potential (see SM for details [55]). In the Born approximation scheme, multiple scatterings are only included on the same impurity [58]. Thus, quantum effects such as interference between different impurities are not taken into consideration. The main physics can be understood by the renormalization of the mass term which occurs due to disorder. This renormalization can change a positive mass term to a negative one, which corresponds to a trivial to nontrivial topological transition. Following two scenarios presented in the original proposal to achieve the QAH effect via magnetic doping of TI thin films [6], herein we compare $(\mathrm{Bi}, \mathrm{Sb})_2\mathrm{Te}_3$ thin films with different thicknesses. Due to quantum confinement, their 2D topological properties are determined by their thickness [27,59]. We compare a thin film with a thickness of 3QLs, which is trivial in the clean and undoped limit, to a film with a thickness of 4QLs being in the QSH state under the same condition. The doping of magnetic ions, such as Cr and V, stabilizes long-range FM order in the 2D bulk states [7,16], and the controllable exchange field gM can drive both of the two kinds of thin films to the QAH phase [6]. In our simulations, one QL is about 1 nm thick and we use the effective parameters specific to $(\mathrm{Bi}, \mathrm{Sb})_2\mathrm{Te}_3$ films from Ref. [28] for the Hamiltonian shown in Eq. (1).

III. DISORDER INDUCED TPT IN MAGNETIC THIN FILMS

Figure 2 summarizes the phase diagram obtained from the conductance G and the corresponding standard deviation δG with respect to exchange field gM and disorder strength W both for magnetically doped TI thin films with thickness of 3QLs and 4QLs when the Fermi energy is located inside the intrinsic band gap. Our work focuses on the effects of disorder, but to paint the full picture we first discuss the $W = 0$ limit and then systematically include the disorder. At zero exchange field 3QLs and 4QLs can be viewed as tokens of two generic classes, either featuring a trivial NI or QSH state. In the case

of a finite exchange field, time reversal symmetry is broken. The QSH state turns to a spin-Chern insulator [53,60], but the NI remains trivial in small enough exchange field. At larger exchange fields a transition to a QAH phase is found for both 3QLs and 4QLs. The NI, QAH, and QSH or spin-Chern insulators are characterized by a quantized conductance of $G = 0$ (white), $G = e^2/h$ (orange), and $G = 2e^2/h$ (green), respectively, in Figs. 2(a) and 2(b). Quantized conductance reflects in vanishing standard deviations in these regions as shown in Figs. 2(c) and 2(d). Still for clean samples, we show the bulk gap in dependence of exchange field in Figs. 2(e) and 2(f). The bulk bands around the Γ point are sketched above as subpanels. The background color indicates different topological phases. By increasing the exchange field in magnitude, the two cases will host a QAH phase with the same Chern number, but the inverted bands belong to different blocks in the Hamiltonian Eq. (1), because the exchange field either inverts one of the formerly trivial bands to a topological one (3QLs) or inverts one topological to a trivial one (4QLs).

We now turn to finite disorder and first concentrate on $gM = 0$. For the 3QL case we find a phase transition driven by disorder from the NI phase to the QSH state akin to the emergence of a TAI [48,49]. While for 4QLs the intrinsic QSH phase survives at finite disorder first, it turns to a trivial Anderson insulator at larger disorder, which happens for each of the scenarios considered in the following at increased disorder strength and therefore we will omit this transition in the following discussion. To discuss this strong disorder phase boundary, a scaling analysis as done in Ref. [49] can be performed. This is, however, beyond the scope of this work. A similar observation holds for the 4QLs case at large enough ($|gM| > 40$ meV); see Figs. 2(b) and 2(d), when the clean system is in the QAH phase. Here, the disorder induced transition can drive a QAH state to spin-Chern insulator. All of the transitions in the weak disorder region are convincingly reproduced by a self-consistent Born approximation shown as lines in the phase diagrams (see SM [55]). Although the QAH effect can be realized both in 3QLs and 4QLs TI thin films, their phase boundaries behave differently as disorder strength is increased. In the magnetically doped TI thin films with 3QLs, weak disorder stabilizes the QAH state, which suggests that the critical value of exchange field to induce the QAH effect becomes smaller when we increase the disorder strength. A similar behavior was reported for the quantum Hall effect [61]. In contrast, for 4QLs thin films, weak disorder stabilizes the spin-Chern insulating phase and a larger exchange field is required to induce the QAH effect compared to the clean sample. These discoveries may help to distinguish the two possible scenarios to achieve the QAH state experimentally [6].

We further examine the phase diagrams as a function of disorder strength W and tuning the Fermi energy E_F for 3QLs magnetically doped TI thin films (for 4QLs see SM [55]). The results are summarized in Fig. 3. At vanishing exchange field, shown in 3(a) and 3(b), we find that the disorder decreases the band gap of the thin film, driving it to be metallic. Further enhancing the disorder potential, a topologically nontrivial TAI state emerges from the NI state. Such a TPT is indicated by the conductance G changing from 0 to 2 (e^2/h) and the standard deviation δG vanishing in these regions (the nondisordered
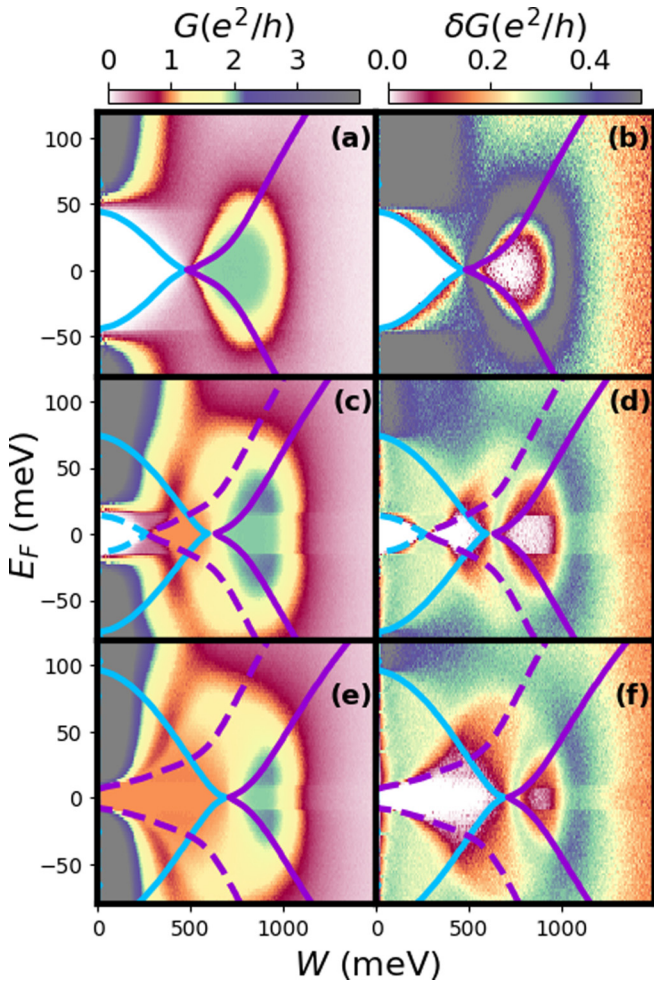
FIG. 3. Left (a),(c),(e) and right (b),(d),(f) panels show the average conductance G and the corresponding standard deviation δG, respectively, as a function of disorder strength W and Fermi energy E_F for 3QLs (Bi, Sb)$_2$Te$_3$ thin film with and without magnetic doping. The exchange fields gM are taken to be (a),(b): 0 meV, (c),(d): 30 meV, and (e),(f): 52 meV. The color lines stand for phase boundaries from self-consistent Born approximation. Details of the colored lines and calculation parameters are shown in Ref. [54]. The system sizes are $L_x = 400a$ for all panels and $L_y = 100a$ for (a),(b) and $L_y = 200a$ for (c)–(f). The disorder average is taken over 500 random configurations.

system corresponds to the point D of (e) in Fig. 2). The phase boundary curve obtained from the self-consistent Born approximation shows excellent agreement with the full calculations. Our discoveries are consistent with previous discussions about HgTe/CdTe quantum wells [48,49].

Next, we turn to finite exchange field in panels (c),(d) and (e),(f) with $gM = 30$ meV and $gM = 52$ meV, whose intrinsic states without disorder belong to the NI and QAH phases, respectively. For the NI state shown in panels (c) and (d), the time reversal symmetry is broken by the long-range FM order, but the exchange field is not strong enough to drive the thin film to be a Chern insulator; it is a trivial dilute magnetic semiconductor. Increasing the disorder strength, the band gap of the thin film becomes smaller in the weak disorder region. Eventually, it closes at the critical value $W_c \approx 290$ meV

and re-opens again, at which point G assumes the quantized value e^2/h and δG is zero, indicating the emergence of a QAH state driven by disorder. More interestingly, when we further enhance the disorder potential, the TI thin film first turns metallic again and then becomes a spin-Chern insulator ($G = 2e^2/h$ and $\delta G = 0$). The weak disorder part of our observations can again be well understood by the self-consistent Born approximation given as lines (see SM [55] for details). Increasing the disorder potential first induces a band closing for the lower block Hamiltonian in the weak disorder region ($W_{c,1} \approx 290$ meV) and then for higher disorder for the upper block Hamiltonian ($W_{c,2} \approx 670$ meV). Consequently disorder tunes TI thin films through a series of phase transitions from NI → QAH → spin-Chern insulator. Similar transitions were reported for less material-oriented toy models before, for example strongly spin-orbit coupled graphene lattices with AFM order [62] and the Lieb lattice [63], which, however, have little possibility to be realized from a real materials' point of view.

In Figs. 3(e) and 3(f), the exchange field is strong enough such that the system is in a QAH phase at $W = 0$ [corresponding to A and G in the subpanels of Fig. 2(e)]. In this case increasing the disorder widens the QAH phase, because the band gap in the lower block Hamiltonian with negative mass is increased by the disorder induced renormalization (see SM for details [55]). For the upper block Hamiltonian whose mass term is positive at $W = 0$, the disorder will decrease the band gap. At a critical disorder strength of $W_c \approx 780$ meV, we observe band inversion, indicating a TPT from the QAH to the spin-Chern insulator phase. The band evolution processes in this system are again captured well within the self-consistent Born approximation at small disorder (see SM for details [55]). We connect our results directly to the experimental findings of Ref. [20], which reports a phase transition from a QAH to a mixed QAH plus metallic states in V-doped (Bi, Sb)$_2$Te$_3$ thin films by changing the gate voltage. Sweeps in the gate voltage correspond to vertical cuts in Fig. 3, and the experimental transition is consistent with the behavior observed around $W = 500$ meV in panels (c) and (e) [with corresponding panels (d) and (f)]. In our theoretical results starting from $E_F = 0$ in the QAH state with finite disorder, one can tune into a regime where G is in between 1 and 2 quantized conductance (yellow color), but the standard deviations δG are still quite suppressed (red color), by increasing E_F. This is a mixed state with properties in between the QAH and a metallic phase.

IV. CONCLUSION

We summarize that in all phase diagrams, non-time-reversal-breaking disorder tends to promote the topological character, and once the material achieves a QSH or spin-Chern insulator state, for which both bands show a topological character, by increasing disorder, it cannot be driven into another topological state, but only into an Anderson insulator. This observation is consistent with the negative contribution to the renormalization of the topological mass term found from the solution of the non-self-consistent Born approximation (see SM [55]). With this, our work puts disordered thin films of magnetically doped (Bi, Sb)$_2$Te$_3$ at the forefront of condensed matter research with a number of interesting TPTs to be

[1] R. S. K. Mong, A. M. Essin, and J. E. Moore, Phys. Rev. B **81**, 245209 (2010).

[2] M. M. Otrokov, I. I. Klimovskikh, H. Bentmann, D. Estyunin, A. Zeugner, Z. S. Aliev, S. Gaß, A. Wolter, A. Koroleva, A. M. Shikin *et al.*, Nature (London) **576**, 416 (2019).

[3] J. Li, Y. Li, S. Du, Z. Wang, B.-L. Gu, S.-C. Zhang, K. He, W. Duan, and Y. Xu, Sci. Adv. **5**, eaaw5685 (2019).

[4] P. Tang, Q. Zhou, G. Xu, and S.-C. Zhang, Nat. Phys. **12**, 1100 (2016).

[5] N. P. Armitage, E. J. Mele, and A. Vishwanath, Rev. Mod. Phys. **90**, 015001 (2018).

[6] R. Yu, W. Zhang, H.-J. Zhang, S.-C. Zhang, X. Dai, and Z. Fang, Science **329**, 61 (2010).

[7] C.-Z. Chang, J. Zhang, X. Feng, J. Shen, Z. Zhang, M. Guo, K. Li, Y. Ou, P. Wei, L.-L. Wang *et al.*, Science **340**, 167 (2013).

[8] C.-X. Liu, S.-C. Zhang, and X.-L. Qi, Annu. Rev. Condens. Matter Phys. **7**, 301 (2016).

[9] K. He, Y. Wang, and Q.-K. Xue, Annu. Rev. Condens. Matter Phys. **9**, 329 (2018).

[10] C.-Z. Chang, J. Zhang, M. Liu, Z. Zhang, X. Feng, K. Li, L.-L. Wang, X. Chen, X. Dai, Z. Fang, X.-L. Qi, S.-C. Zhang, Y. Wang, K. He, X.-C. Ma, and Q.-K. Xue, Adv. Mater. **25**, 1065 (2013).

[11] J. Zhang, C.-Z. Chang, P. Tang, Z. Zhang, X. Feng, K. Li, L.-l. Wang, X. Chen, C. Liu, W. Duan *et al.*, Science **339**, 1582 (2013).

[12] A. L. Sharpe, E. J. Fox, A. W. Barnard, J. Finney, K. Watanabe, T. Taniguchi, M. Kastner, and D. Goldhaber-Gordon, Science **365**, 605 (2019).

[13] M. Serlin, C. Tschirhart, H. Polshyn, Y. Zhang, J. Zhu, K. Watanabe, T. Taniguchi, L. Balents, and A. Young, Science **367**, 900 (2020).

[14] Y. Deng, Y. Yu, M. Z. Shi, Z. Guo, Z. Xu, J. Wang, X. H. Chen, and Y. Zhang, Science **367**, 895 (2020).

[15] J. G. Checkelsky, R. Yoshimi, A. Tsukazaki, K. S. Takahashi, Y. Kozuka, J. Falson, M. Kawasaki, and Y. Tokura, Nat. Phys. **10**, 731 (2014).

[16] C.-Z. Chang, W. Zhao, D. Y. Kim, H. Zhang, B. A. Assaf, D. Heiman, S.-C. Zhang, C. Liu, M. H. Chan, and J. S. Moodera, Nat. Mater. **14**, 473 (2015).

[17] Y. Feng, X. Feng, Y. Ou, J. Wang, C. Liu, L. Zhang, D. Zhao, G. Jiang, S.-C. Zhang, K. He, X. Ma, Q.-K. Xue, and Y. Wang, Phys. Rev. Lett. **115**, 126801 (2015).

[18] X. Kou, S.-T. Guo, Y. Fan, L. Pan, M. Lang, Y. Jiang, Q. Shao, T. Nie, K. Murata, J. Tang, Y. Wang, L. He, T.-K. Lee, W.-L. Lee, and K. L. Wang, Phys. Rev. Lett. **113**, 137201 (2014).

[19] A. J. Bestwick, E. J. Fox, X. Kou, L. Pan, K. L. Wang, and D. Goldhaber-Gordon, Phys. Rev. Lett. **114**, 187201 (2015).

[20] C.-Z. Chang, W. Zhao, J. Li, J. K. Jain, C. Liu, J. S. Moodera, and M. H. W. Chan, Phys. Rev. Lett. **117**, 126802 (2016).

[21] K. Yasuda, M. Mogi, R. Yoshimi, A. Tsukazaki, K. S. Takahashi, M. Kawasaki, F. Kagawa, and Y. Tokura, Science **358**, 1311 (2017).

[22] M. Mogi, R. Yoshimi, A. Tsukazaki, K. Yasuda, Y. Kozuka, K. Takahashi, M. Kawasaki, and Y. Tokura, Appl. Phys. Lett. **107**, 182401 (2015).

[23] Q. Liu, C.-X. Liu, C. Xu, X.-L. Qi, and S.-C. Zhang, Phys. Rev. Lett. **102**, 156603 (2009).

[24] J. G. Checkelsky, J. Ye, Y. Onose, Y. Iwasa, and Y. Tokura, Nat. Phys. **8**, 729 (2012).

[25] J.-J. Zhu, D.-X. Yao, S.-C. Zhang, and K. Chang, Phys. Rev. Lett. **106**, 097201 (2011).

[26] C.-Z. Chang, P. Tang, Y.-L. Wang, X. Feng, K. Li, Z. Zhang, Y. Wang, L.-L. Wang, X. Chen, C. Liu, W. Duan, K. He, X.-C. Ma, and Q.-K. Xue, Phys. Rev. Lett. **112**, 056801 (2014).

[27] K. He, Y. Zhang, K. He, C. Z. Chang, C. L. Song, L. L. Wang, X. Chen, J. F. Jia, Z. Fang, and X. Dai, Nat. Phys. **6**, 712 (2010).

[28] J. Wang, B. Lian, and S.-C. Zhang, Phys. Rev. Lett. **115**, 036805 (2015).

[29] Z. Zhang, X. Feng, J. Wang, B. Lian, J. Zhang, C. Chang, M. Guo, Y. Ou, Y. Feng, S.-C. Zhang *et al.*, Nat. Nano. **12**, 953 (2017).

[30] K. Nomura and N. Nagaosa, Phys. Rev. Lett. **106**, 166802 (2011).

[31] H.-Z. Lu, J. Shi, and S.-Q. Shen, Phys. Rev. Lett. **107**, 076801 (2011).

[32] Z. Qiao, Y. Han, L. Zhang, K. Wang, X. Deng, H. Jiang, S. A. Yang, J. Wang, and Q. Niu, Phys. Rev. Lett. **117**, 056802 (2016).

[33] C.-Z. Chen, H. Liu, and X. C. Xie, Phys. Rev. Lett. **122**, 026601 (2019).

[34] A. Haim, R. Ilan, and J. Alicea, Phys. Rev. Lett. **123**, 046801 (2019).

[35] Y. Xing, F. Xu, K. T. Cheung, Q.-f. Sun, J. Wang, and Y. Yao, New J. Phys. **20**, 043011 (2018).

[36] J. Wang, B. Lian, and S.-C. Zhang, Phys. Rev. B **89**, 085106 (2014).

[37] A. C. Keser, R. Raimondi, and D. Culcer, Phys. Rev. Lett. **123**, 126603 (2019).

[38] W. Wang, Y. Ou, C. Liu, Y. Wang, K. He, Q.-K. Xue, and W. Wu, Nat. Phys. **14**, 791 (2018).

[39] I. Lee, C. K. Kim, J. Lee, S. J. Billinge, R. Zhong, J. A. Schneeloch, T. Liu, T. Valla, J. M. Tranquada, G. Gu *et al.*, Proc. Natl. Acad. Sci. USA **112**, 1316 (2015).

[40] E. O. Lachman, A. F. Young, A. Richardella, J. Cuppens, H. Naren, Y. Anahory, A. Y. Meltzer, A. Kandala, S. Kempinger, Y. Myasoedov *et al.*, Sci. Adv. **1**, e1500740 (2015).

[41] X. Kou, L. Pan, J. Wang, Y. Fan, E. S. Choi, W.-L. Lee, T. Nie, K. Murata, Q. Shao, S.-C. Zhang *et al.*, Nat. Commun. **6**, 8474 (2015).

[42] Z.-Q. Zhang, C.-Z. Chen, Y. Wu, H. Jiang, J. Liu, Q. feng Sun, and X. C. Xie, arXiv:2007.07619.

[43] L. A. Wray, S.-Y. Xu, Y. Xia, D. Hsieh, A. V. Fedorov, Y. San Hor, R. J. Cava, A. Bansil, H. Lin, and M. Z. Hasan, Nat. Phys. **7**, 32 (2011).

[44] Y. Yuan, X. Wang, H. Li, J. Li, Y. Ji, Z. Hao, Y. Wu, K. He, Y. Wang, Y. Xu, W. Duan, W. Li, and Q.-K. Xue, Nano Lett. **20**, 3271 (2020).

[45] C. Chen, M. Teague, L. He, X. Kou, M. Lang, W. Fan, N. Woodward, K. Wang, and N. Yeh, New J. Phys. **17**, 113042 (2015).

[46] J. Liao, Y. Ou, X. Feng, S. Yang, C. Lin, W. Yang, K. Wu, K. He, X. Ma, Q.-K. Xue, and Y. Li, Phys. Rev. Lett. **114**, 216601 (2015).

[47] X. Wu, D. Xiao, C.-Z. Chen, J. Sun, L. Zhang, M. H. W. Chan, N. Samarth, X. C. Xie, X. Lin, and C.-Z. Chang, Nat. Commun. **11**, 4532 (2020).

[48] J. Li, R.-L. Chu, J. K. Jain, and S.-Q. Shen, Phys. Rev. Lett. **102**, 136806 (2009).

[49] C. W. Groth, M. Wimmer, A. R. Akhmerov, J. Tworzydło, and C. W. J. Beenakker, Phys. Rev. Lett. **103**, 196805 (2009).

[50] H. Jiang, L. Wang, Q.-f. Sun, and X. C. Xie, Phys. Rev. B **80**, 165316 (2009).

[51] A. Yamakage, K. Nomura, K.-I. Imura, and Y. Kuramoto, Phys. Rev. B **87**, 205141 (2013).

[52] J. Song, H. Liu, H. Jiang, Q.-f. Sun, and X. C. Xie, Phys. Rev. B **85**, 195125 (2012).

[53] D. N. Sheng, Z. Y. Weng, L. Sheng, and F. D. M. Haldane, Phys. Rev. Lett. **97**, 036808 (2006).

[54] The parameters in simulations are $v_F = 3.07/2.36$ eV Å, $m_0 = 44/-29$ meV, $B = 37.3/12.9$ eV Å^2 for (Bi, Sb)$_2$Te$_3$ thin film with thickness of 3QLs/4QLs [28]. Solid and dashed lines correspond to phase boundaries calculated from the self-consistent Born approximation for the upper and lower block of the Hamiltonian. The blue and purple lines show $|\overline{\mu}^{u/l}| = \overline{m}_0^{u/l}$ and $|\overline{\mu}^{u/l}| = -\overline{m}_0^{u/l}$, respectively.

[55] See Supplemental Material at http://link.aps.org/supplemental/10.1103/PhysRevB.102.201405 for details about the Born approximation, lead effect, and the topological phase transition driven by disorder for 4QLs.

[56] R. Landauer, Philos. Mag. **21**, 863 (1970).

[57] M. Büttiker, Phys. Rev. B **38**, 9375 (1988).

[58] H. Bruus and K. Flensberg, *Many-Body Quantum Theory in Condensed Matter Physics - An Introduction* (Oxford University Press, Oxford, 2004).

[59] C.-X. Liu, H. Zhang, B. Yan, X.-L. Qi, T. Frauenheim, X. Dai, Z. Fang, and S.-C. Zhang, Phys. Rev. B **81**, 041307(R) (2010).

[60] The spin-Chern number is defined in orbital space instead of real spin space.

[61] P. A. Lee and T. V. Ramakrishnan, Rev. Mod. Phys. **57**, 287 (1985).

[62] Y. Su, Y. Avishai, and X. R. Wang, Phys. Rev. B **93**, 214206 (2016).

[63] R. Chen, D.-H. Xu, and B. Zhou, Phys. Rev. B **96**, 205304 (2017).

[64] Takuya Okugawa, Peizhe Tang, Angel Rubio, and Dante M. Kennes (unpublished).